Geobarometry of mafic and ultramafic xenoliths: examples from Hualalai and Mauna Kea volcanoes, Hawaii

Ziberna, L.

Department of Mathematics and Geosciences, University of Trieste, Italy

Email: luca.ziberna@units.it

Index terms

3612, 3618, 3640, 3651, 3037

Keywords

Pressure, Gabbro, Hawaii, Seismic velocities, Phase equilibria

Short running title

Geobarometry of mafic and ultramafic xenoliths

Abstract

Xenoliths of plutonic rocks sporadically torn off by erupting magmas are known to carry valuable information about volcano plumbing systems and the lithosphere in which they emplace. One of the main steps to interpret such information is to quantify the pressure and temperature conditions at which the xenolith mineral assemblages last equilibrated. This chapter discusses some aspects of geothermobarometry of mafic and ultramafic rocks using the xenolith populations of Hualalai and Mauna Kea volcanoes, Hawaii, as case studies. Multiple-reaction geobarometry, recently revisited for olivine + clinopyroxene + plagioclase ± spinel assemblages, provides the most precise pressure estimates (uncertainties as low as 1.0 kbar). An example is shown that integrates these estimates with calculated seismic velocities of the xenoliths and the available data from seismic tomography. The results allow to better constrain some km-scale horizontal and vertical heterogeneities in the magmatic system beneath Hawaii. Ultramafic xenoliths at Hualalai are the residuals of magma crystallization at 16–21 km depth,

below the pre-Hawaiian oceanic crust. Few available gabbronorites and diorites record instead lower pressures and likely represent conduits or small magma reservoir crystallized at 0–8 km depth. At Mauna Kea, on the other hand, a significant portion of the xenolith record is composed by olivine-gabbros, which crystallized almost over the entire crustal thickness (3–18 km). Ultramafic xenoliths are less abundant and might represent the bottom of the same magma reservoirs that crystallized in the deeper portion of the magmatic systems (11–18 km). Some unresolved issues remain in geothermometry of mafic and ultramafic rocks representing portions of magma reservoirs that cooled and recrystallized under subsolidus conditions. This suggests that further experimental and theoretical work is needed to better constrain the thermodynamics and kinetics of peridotitic and basaltic systems at low (< 1000˚C) temperatures.

1 Introduction

Geothermobarometry of magmatic rocks is well known to be one of the key tools to interpreting the processes within volcanic systems. This is why much effort has been spent since the first pioneering studies in petrology (e.g., Bowen, 1928; Green & Ringwood, 1967; Tuttle & Bowen, 1958; Wells, 1970) to perform experimental and theoretical work constraining the relationships between mineralogy and chemistry of magmatic rocks and temperatures and pressures at which their constituent phases formed. It was clear since then that the complexity of volcanic processes and the compositional variability of the erupted magmas and their lithic fragments make it difficult to develop geothermobarometers that are both accurate and precise for any sample, but considerable progress has been made in the last three decades. Considering only published work in magmatic systems relevant for crustal processes, more than six thousand phase equilibrium laboratory experiments have been perfomed so far (based on the LEPR database at http://lepr.ofm-research.org and additional literature). These experiments led to the development of geothermobarometers and forward thermodynamic simulations (e.g.,

Ghiorso & Sack, 1995; Gualda et al., 2012; Jennings & Holland, 2015; Masotta et al., 2013; Mollo et al., 2018; Putirka, 2008, 2016; Ziberna et al., 2017) that can now be used to model the differentiation paths of magmas.

The most common inverse-modelling approach to estimate the pressure (*P*) and temperature (*T*) of volcanic systems is geothermobarometry based on mineral-liquid equilibria (see Putirka, 2008, for an exhaustive discussion). It is usually applied to porphyric lava samples, using whole-rock chemical analyses (as representative of liquid compositions) in combination with the chemistry of phenocrysts. As a rule, measured partition coefficients [e.g., $K_D(Fe\text{-}Mg)^{mineral\text{-}liquid}$] is compared to experimental values to demonstrate equilibrium (e.g., Putirka, 2008). For basaltic to andesitic and trachytic rocks, clinopyroxene-liquid geothermometry and geobarometry showed to be the most precise methods when tested against experimental data, producing model errors as small as 28 ˚C and 1.4 kbar (Masotta et al., 2013; Neave & Putirka, 2017; Putirka, 2008). The success of such methods lies on the large entropy and volume change of the reactions used as geothermometers and geobarometers, respectively (Putirka, 2008), and on the ubiquity of clinopyroxene in many basaltic systems. Other common methods are plagioclase-liquid geothermometry (e.g., Lange et al., 2009; Putirka, 2008), amphibole-liquid geothermometry and geobarometry (Molina et al., 2015; Putirka, 2016), and mineral-mineral equilibria like two-pyroxenes geothermometers and geobarometers (e.g., Lindsley, 1983; Putirka, 2008; Wells, 1977), amphibole-plagioclase geothermometers (Blundy & Holland, 1990; Holland & Blundy, 1994) and geobarometers (Molina et al., 2015), Ca-in-olivine geothermometers (Shejwalkar & Coogan, 2013) or two-oxides geothermometers (Ghiorso & Evans, 2008). Furthermore, new methods based on the partitioning of rare earth elements (REEs) are the two-pyroxenes thermometer of Liang et al. (2013) and the plagioclase-clinopyroxene thermometer of Sun and Liang (2017).

Phenocryst assemblages in volcanic rocks often show complex intra- and inter-mineral variations in major and trace element compositions (i.e., zoning and grain-to-grain heterogeneities), which are known to reflect possible changes in P, T, oxygen fugacity (fO_2), undercooling, degassing, crystallization and interaction with other magmas or crustal rocks. Application of mineral-liquid geothermobarometers to such assemblages is not a straightforward task, but recent careful studies taking into account the textural relationships in lavas and the required care for assessing equilibrium have shown that these methods can help investigating the complex architecture of magmatic systems (e.g., Erdmann et al., 2014; Giacomoni et al., 2016; Mollo et al., 2015, 2020; Neave et al., 2019; Putirka, 1997; Stock et al., 2018).

Erupted lavas, however, represent only part of volcano plumbing systems and do not provide direct information about the residua of crystal fractionation (i.e., cumulates) or plutonic rocks derived from isochemical solidification of magmas at depth. Such information is rather provided by plutonic or cumulate xenoliths that are occasionally brought to the surface by the erupted magmas. These are valuable samples that can be studied in combination with volcanic rocks to unravel magmatic processes at depth and help constraining the crustal structure beneath volcanoes. In most cases, classical mineral-liquid geothermobarometers cannot be applied to these rocks, either because the liquid composition is not well constrained or because the system re-equilibrated at subsolidus conditions. The available methods are therefore based on either single-reactions between mineral phases (e.g., two-pyroxenes geothermobarometry; Putirka, 2008; olivine-plagioclase-pyroxenes geobarometry; Fumagalli et al., 2017), REE-partitioning (Liang et al., 2013; Sun & Liang, 2015; Sun & Liang, 2017) or on multiple-reaction approaches (e.g., Powell & Holland, 1994) using as many mineral phases as those present in the assemblage and for which thermodynamic data are available.

Obtaining accurate pressure estimates for mafic and ultramafic plutonic xenolith has always been hampered by the lack of suitable geobarometers with sufficiently large volume change of their reactions. While the problem still remains for rocks with high variance assemblages, like pure dunites, clinopyroxenites, wehrlites and troctolites with no accessory phases, recent work showed that obtaining accurate and precise pressure estimates for lower variance assemblages is possible by means of either a single-reaction ($Mg_2SiO_4^{olivine}$ + $CaAl_2Si_2O_8^{plagioclase}$ = $CaAl_2SiO_6^{clinopyroxene}$ + $Mg_2Si_2O_6^{orthopyroxene}$; Fumagalli et al., 2017) or a multiple-reaction approach (three or six reactions in the assemblage olivine + clinopyroxene + plagioclase ± spinel; Ziberna et al., 2017). The multiple-reaction approach relies on an internally consistent dataset of thermodynamic data for mineral end-members (e.g., Holland & Powell, 2011) and a set of mixing models for phases. In principle, it allows for all the phases in a rock to be used for P calculations and is based on an algorithm (i.e., average *P*, *avP*, originally developed for metamorphic rocks, Powell & Holland, 1994) that combines all the thermodynamic information and takes into account uncertainties and correlations of the input data (mineral composition, thermodynamic properties) to produce an average value of *P*. The *avP* method has been tested and refined for olivine-bearing igneous rocks and has been shown to accurately reproduce the pressure of phase equilibrium experiments and produce *P* estimates for natural samples with 1σ uncertainties on the order of 1 kbar (Ziberna et al., 2017).

The objective of this chapter is to show how geobarometry can help constraining the depth of formation of mafic and ultramafic xenoliths brought to the surface at basaltic volcanoes. As an example application, I selected the Hualalai and Mauna Kea volcanoes of the island of Hawaii, which erupted a large quantity of ultramafic and mafic xenoliths that have been variably characterized by the petrological community. I will illustrate some advantages and limitations of some available geothermobarometers and how their results can be reconciled with the seismic structure of the crust beneath hot spot volcanoes.

2 Geological and petrological background

Hualalai and Mauna Kea are two of the five volcanoes that build up the island of Hawaii (Fig. 1). Similarly to other volcanoes from this island, their erupting activity can mainly be subdivided in a tholeiitic shield stage and an alkalic post-shield or post-caldera stage (Clague, 1987). The tholeiitic shield stage produced most of the erupted volumes and at Mauna Kea is suggested to have started at ~ 600 ka (Frey et al., 1990). The shield to postshield transition is dated around 370 ka for Mauna Kea (Huang & Frey, 2003; Vazquez et al., 2007) and between 130 and 100 ka for Hualalai (Cousens et al., 2003). The most recent erupted products are some lava flows of the Laupahoehoe volcanics (~ 4 ka) at Mauna Kea (Wolfe et al., 1997) and the 1800-1801 Huehue and Kaupulehu lava flows at Hualalai (Clague et al., 1980). Reviews on Mauna Kea and Hualalai volcanism can be found in Frey et al. (1990, 1991), Moore et al. (1987) and Wolfe et al. (1997).

Both Hualalai and Mauna Kea eruptions of the postshield stage brought to the surface crustal and more rarely mantle xenoliths that have been variably characterized by the petrological community (e.g., Bohrson & Clague, 1998; Chen et al., 1992; Fodor & Galar, 1997; Jackson et al., 1981, 1982; Shamberger & Hammer 2006). More than four thousands xenoliths, ranging in size from ~1 cm to more than 40 cm, have been reported so far; rock types include dunites, wehrlites, clinopyroxenites, gabbros, gabbronorites, troctolites and minor anorthosites, diorites and tonalities (e.g., Chen et al., 1992; Clague & Bohrson, 1991; Fodor, 2001; Fodor & Vandermeyden, 1988; Gao et al., 2016; Jackson et al., 1981, 1982; Shamberger & Hammer, 2006). Only a small part has been characterized for detailed petrography and mineral chemistry. With the exception of few diorites and gabbros (Fodor, 2001; Gao et al., 2016; Shamberger & Hammer, 2006), all xenoliths have been interpreted as fragments of cumulates derived by crystallization of Hawaiian tholeiitic and/or alkalic magmas (Bohrson & Clague, 1988; Fodor & Galar, 1997; Fodor & Vandermeyden, 1988). Based on Sr and Pb isotopic

compositions and mineral chemistry of the xenoliths, derivation from the pre-Hawaiian oceanic crust has been excluded for most of the xenoliths (Bohrson & Clague, 1988; Fodor & Galar, 1997; Shamberger & Hammer, 2006). Most of the ultramafic xenoliths show evidence of annealing or recrystallization (Fodor & Galar, 1997), but this is not the case for the leucocratic and most of the gabbroic types (Shamberger & Hammer, 2006). Textures and composition of the ultramafic xenoliths suggest that they formed in bottoms of reservoirs from magmas having 10–15 wt% MgO (Fodor & Galar, 1997).

Previous work generally suggests that both small- and large-scale modal, grain size and phase layering is a common feature of magma reservoirs beneath Hawaii (e.g., Fodor & Galar, 1997). While small (cm)-scale layering is evidenced by the occurrence of composite xenoliths (c.f. Fodor & Galar, 1997; Hoover & Fodor, 1997), possible large (km)-scale layering is more difficult to constrain. In principle, precise pressure estimates of the xenoliths could provide insights on this inferred layering, and more generally on the architecture of the magmatic system beneath Hawaii. However, most common geobarometers applicable to the xenoliths are affected by uncertainties of ~3 kbar (e.g., two-pyroxenes barometer; Putirka et al., 2008), which propagate on depth uncertainties of ~10 km. Considering that the crustal thickness in Hawaii is lower than 20 km (Park et al., 2009; Zucca et al., 1982), such uncertainties are too high to well constrain any km-scale heterogeneity. The recently refined multiple-reaction geobarometer for clinopyroxene + olivine + plagioclase assemblages (Ziberna et al., 2017), which has been shown to have pressure uncertainties as small as 1.0 kbar, might provide a new opportunity to overcome this issue.

3 Revised geothermobarometry of Mauna Kea and Hualalai xenoliths

3.1 Rationale and data selection

There are several aspects to bear in mind when selecting a set of geothermometers and geobarometers to be applied to a xenolith population. i) The selection is clearly restricted to

algorithms involving phases that are present in the xenolith assemblage. For a xenolith suite composed by different lithologies, this often leads to the application of different geothermometers or geobarometers. If these were calibrated on different experimental datasets, their application might produce potentially inconsistent results. ii) The compositions of the phases have to be reasonably assumed to represent equilibrium conditions. iii) When the thermodynamic data of a given thermobarometric algorithm have been simplified to few parameters and these parameters have been calibrated from experiments in a specific range of pressures, temperatures, compositions and phase assemblages, then its application outside this range must be taken with caution. iv) Model errors (i.e., errors calculated from regression statistics on a test experimental dataset) of a thermobarometer derived as in (iii) represent only minimum errors when the algorithm is applied to natural assemblages. Additional, potentially quantifiable errors might derive from propagation of analytical errors that are higher than the average errors of the experimental dataset used for calibration. Further, unquantifiable errors might instead rise if compositions do not represent complete equilibrium conditions, despite assumption (ii), and if simplified thermodynamic equations are applied outside the P-T-x range of experimental calibration [aspect (iii)]. Notably, the concept of model errors as defined above is not applied to a multiple-reaction approach like the *avP* method (Powell & Holland, 1994; Ziberna et al., 2017). In this case, errors are calculated by propagation of uncertainties on both mineral compositions and thermodynamic properties of end-members of phases, taking into account the correlations between reactions that share end-members.

The method that recently showed to predict the pressures of phase equilibrium experiments with sufficient accuracy and that can be applied to a discrete part of the xenolith suite from Hualalai and Mauna Kea is the *avP* method refined for olivine-bearing assemblages (Ziberna et al., 2017). Pressures have been therefore calculated with this method, with a major focus given to spinel + clinopyroxene + olivine + plagioclase (SCOlP) assemblages, which allows

using six reactions in the averaging procedure (Ziberna et al., 2017). Temperatures have been calculated with Ca-in-olivine geothermometry, which is convenient for applications to olivine+clinopyroxene-bearing assemblages. Available algorithms include those of Kohler & Brey (1990), which however were calibrated in peridotitic systems with olivines with $Fo_{87–100}$, not resembling the compositions of the Hawaiian xenoliths examined in this study (Fo_{67-86}). Moreover, their dataset used for calibration includes experiments performed at P = 10–60 kbar (with the exception of one experiment at 2 kbar), which is outside the P range expected for Hawaiian xenoliths (P = 0–8 kbar; e.g., Bohrson & Clague, 1988; Shamberger & Hammer 2006). I have therefore selected the method of Shejwalkar and Coogan (2013), which was calibrated in basaltic systems for olivines with $Fo_{70–100}$, closer to the compositional range of Hawaiian xenoliths. Still, their experiments used for calibrations are at P = 0.001 kbar and T = 1170–1322 ˚C, and therefore its results must be taken with caution [see aspect (iii) above and discussion in section 2.2]. For the sake of comparison, pressures and temperatures have been calculated using also the two-pyroxenes geobarometer and geobarometer of Putirka (2008; his equations 36 and 39).

For this geothermobarometric study, I selected all the available published datasets on the Hualalai and Mauna Kea xenoliths that include both petrographic characterization and electron microprobe analyses of minerals (Bohrson & Clague, 1988; Chen et al., 1992; Clague & Bohrson, 1991; Fodor, 2001; Fodor & Galar, 1997; Fodor & Vandermeyden, 1988; Hoover & Fodor, 1997; Schamberger & Hammer, 2006). This collection of data includes eighty-five samples from Hualalai and one-hundred-twenty-three xenoliths from Mauna Kea. A first screening has been made to select the xenolith containing the appropriate phases for geothermobarometry (i.e., olivine + clinopyroxene + plagioclase, clinopyroxene + orthopyroxene, or both) and for which chemical composition of these phases are available. Further screening has been made to discard thirteen xenoliths which were described in the

source papers as showing evidence of textural disequilibrium, or that are characterized by large intra-sample compositional variations of pyroxenes {> 0.03 mg#[(Mg/(Mg+Fe^{2+}), Fe^{2+} calculated after Droop, 1987] units}, olivine (> 0.03 mg# units) and/or plagioclase (> 10 mol% of anorthite component). This screening produced a dataset of thirty-one xenoliths from Hualalai and fifty xenoliths from Mauna Kea.

3.2 Temperature estimates

For Hualalai, temperatures calculated with the Ca-in-olivine thermometer ($T_{Ca\text{-}in\text{-}ol}$; eq. 12 in Shejwalkar & Coogan, 2013) range from 997 ˚C to 1168 ˚C (with a major cluster at 1040–1117 ˚C) for the ultramafic xenoliths, and from 841 ˚C to 904 ˚C for gabbroic xenoliths (see Supplementary material and Figs. 2a, 3a). For Mauna Kea, on the other hand, calculated temperatures are indistinguishable between the ultramafics and the gabbroic rocks and are in the range 744–1103 ˚C (see Supplementary material and Figs. 2a, 3a). Two-pyroxenes temperatures ($T_{cpx\text{-}opx}$) show a similar relative difference between Hualalai and Mauna Kea (Figs. 2c,d). However, Figures 2 and 3a show that at lower temperatures (< 1050 ˚C) two-pyroxenes geothermometry produce significantly higher values (up to 230 ˚C; 125 ˚C on average) than Ca-in-olivine geothermometry.

Here I infer that the discrepancy between two-pyroxenes and Ca-in-olivine temperatures could be related to the slower diffusion of Mg-Fe^{2+} in pyroxenes compared to Ca in olivine (Chakraborty, 2010; Cherniak & Dimanov, 2010; Coogan et al., 2005; Müller et al., 2013), which would make in principle the Ca-in-olivine method more suitable for applications to cumulate rocks that underwent cooling below subsolidus temperatures. As a matter of fact, the source of the deviations seen in Fig. 3a is less likely to be related to the calibration strategies of either methods, since a test on a large experimental dataset shows that both methods appear to overestimate experimental values at low temperatures (with more pronounced overestimation by the Ca-in-olivine method; Figs. 3b,c). This is true also when using a tentative

equation for Ca-in-olivine geothermometry that accounts for its pressure dependency (eq. 13 in Shejwalkar & Coogan, 2013; Figs. 3c,d). The sudden change in the deviations of $T_{\text{Ca-in-ol}}$ from T_{exp} shown in Fig. 3c could be related to a change in the solubility mechanism of Ca in olivine at low temperatures (Köhler & Brey, 1990). Note that the test in Figs. 3c,d is shown only as a first, preliminary evaluation, since the experimental dataset does not include data obtained with analytical conditions optimized for analysis of Ca content in olivine, which is indeed reflected by the large deviations of Ca-in-olivine temperatures from experimental values. In addition, there are scarce experimental data at $T < 1000$˚C, and no data at all at $T <$ 900 ˚C, which are the temperatures of interest for investigating the subsolidus conditions of mafic and ultramafic cumulates during cooling.

3.3 Pressure estimates

For Hualalai, pressures calculated with *avP* ($\overline{P}$) on SCOlP assemblages, at temperatures $T_{\text{Ca-in-ol}}$, vary in the range $\overline{P}$ = 5.5–6.7 kbar ($\sigma_{\overline{P}}$ = 0.9–1.2 kbar) for the ultramafic xenoliths, $\overline{P}$ = -0.6–2.6 kbar ($\sigma_{\overline{P}}$ = 1.0–2.0 kbar) for gabbronorites and dioritic xenoliths, and $\overline{P}$ = 5.4 kbar ($\sigma_{\overline{P}}$ = 1.0 kbar) for one gabbro xenolith. For Mauna Kea, the calculated pressures of the different lithologies overlap within the range $\overline{P}$ = 0.6–5.9 kbar ($\sigma_{\overline{P}}$ = 1.0–2.8 kbar). Calculations produced diagnostic σ_{fit} values (Powell & Holland, 1994) that are generally higher for samples from Mauna Kea (σ_{fit} = 1.2–2.7) with respect to Hualalai (σ_{fit} = 0.4–1.8). The cut-off value provided by the χ^2 test, representing 95% confidence of the average P calculations (Powell & Holland, 1994), is $\sigma_{\text{fit}} < 1.49$. However, higher values could still be considered acceptable, since $\sigma_{\overline{P}}$ is increased by a factor equal to σ_{fit} when the χ^2test fails (Ziberna et al., 2017), as shown by the generally higher uncertainties for Mauna Kea samples (Fig. 2b).

Compared to the results of *avP*, application of the two-pyroxenes geobarometer at temperatures $T_{\text{cpx-opx}}$ provides generally higher pressures for Hualalai samples ($P^{\text{cpx-opx}}$ = 6.2–

10.9 kbar for ultramafic xenoliths; 1.4–6.3 kbar for gabbroic and dioritic xenoliths) and similar ranges of pressures for Mauna Kea ($P^{cpx\text{-}opx}$ = -1.7–6.4 kbar). Model error for this geobarometer, as reported in Putirka (2008), is 2.8 kbar (if clinopyroxene mg# > 0.75, which is the case for the dataset considered in this work). Note that, since *avP* and two-pyroxenes geobarometers are based on two different assemblages, they were applied to two partially different subsets of xenoliths. Figure 4 avoids possible misleading interpretations by showing the results of each barometer for the individual xenoliths. This plot confirms that for Hualalai xenoliths the two-pyroxenes geobarometer produces higher pressures than *avP*, as evidenced by the xenolith containing the assemblage olivine + clinopyroxene + orthopyroxene + plagioclase + spinel. On the other hand, pressures estimated with two-pyroxenes and *avP* methods on Mauna Kea xenoliths do not show systematic differences.

To evaluate the effect of temperature on the pressures estimated with *avP*, Figure 4 also includes values of $\overline{P}$ calculated with temperatures from two-pyroxenes thermometry, where possible. With few exceptions, the differences are smaller than 1.2 kbar and are not systematic (Fig. 4). Furthermore, Fig. 4 includes the results of *avP* using the COlP assemblage at $T_{Ca\text{-}in\text{-}ol}$, since some of the olivine-bearing gabbroic xenoliths do not contain spinel. The results are comparable, with a slight *P* overestimation compared to the pressures obtained using the SCOlP assemblage, consistently with the observations of Ziberna et al. (2017). Despite using a SCOlP assemblage is considered more reliable, since it allows using an independent set of six reactions instead of three (Ziberna et al., 2017), the results of *avP* using the COlP assemblage are useful to show that troctolites from Mauna Kea record among the lowest pressures of the xenolith suite (Fig. 4).

4 Discussion

4.1 Comparisons with previous estimates and implications of the results

Compared to the previous estimates on Hawaiian xenoliths, the results obtained with the *avP* method allow for more precise quantification of their pressure of formation and for the xenolith data to be placed in the context of crustal structure of the Hawaiian crust. Based on the model of Wolfe et al. (1997), the top of the ~ 5 km-thick Pacific oceanic crust beneath the island of Hawaii is mostly covered by a ~12 km-thick unit of shield-stage tholeiites. This is illustrated in Fig. 5, a schematic cross-section of the crust beneath Hualalai and Mauna Kea volcanoes. The results of *avP* calculations of each xenolith have been grouped and schematically represented as coloured boxes in Fig. 5, in order to allow a direct comparison between the depth estimates for the xenoliths to the modelled structure of the crust. This comparison might be oversimplified for an in-depth investigation and it is shown here only to demonstrates the potential of precise pressure estimates on xenoliths from active magmatic systems.

Previous estimates for the ultramafic xenoliths from Hualalai were only semi-quantitative and indicated a pressure range of 4.5–9.0 kbar, based on a comparison between the mineralogy of the xenoliths and the results of phase equilibrium experiments and on the minimum trapping pressure of CO_2 inclusions in olivines (Bohrson & Clague, 1988; Chen et al., 1992). *AvP* calculations on the available xenolith data agree with these estimates, but suggest a much narrower range ($\overline{P}$ = 5.5–6.7 kbar), with calculated errors for each xenolith smaller than 1.2 kbar. This pressure range translates to a depth range of 16–21 km b.s.l. (Fig. 5), which is consistent with the presence of a pile of ultramafic cumulates derived from fractionation of basaltic magmas at or below the base of the Pacific oceanic crust, as already suggested by Bohrson & Clague (1988).

For the gabbronorites and diorites from Hualalai, Shamberger and Hammer (2006) suggested that their pressure of formation span anywhere between 2.5 and 7.5 kbar, based on

the application of the single-clinopyroxene method of Nimis (1999) and qualitative comparisons between natural and experimental clinopyroxene compositions. These pressures are higher than the results of *avP* calculations, which rather indicate a pressure range of 0.0–2.6 kbar, and translates to a depth range of 0–8 km (Fig. 5). Since diorites xenoliths are considered parental to the Hualalai trachytes (Shamberger & Hammer, 2006), this depth range supports the hypothesis of trachytes formed by crystal fractionation in a shallow (3–7 km; Clague, 1987; Cousens et al., 2003) rather than deep (10–23 km; Shamberger & Hammer, 2006) reservoirs during the shield to postshield transition. It is worth noting, however, that two-pyroxenes geothermobarometry on ol-free diorites (Fig. 2c) suggests significantly higher pressures ($P^{cpx\text{-}opx}$ = 4.9–6.5 kbar) than the *avP* calculation on the only available ol-bearing diorite ($\overline{P}$ = 2.2 kbar). Further work will be needed to understand if such difference is related to possible inconsistency of the geothermobarometric methods or to an actual difference in the pressure of formation of ol-free and ol-bearing diorites.

As already noted by Clague (1987) and Fodor and Galar (1997), while at Hualalai most of xenoliths are ultramafic, at Mauna Kea the majority of xenoliths are gabbroic. They suggested that this might reflect lower magma-production rates at Mauna Kea, which allowed for more extensive fractionation and production of magmas with FeO/MgO > 2. Fodor and Galar (1997) suggested that the gabbroic and ultramafic xenoliths at Mauna Kea record similar pressures, following the observation of similar Al^{iv}/Al^{vi} ratios in clinopyroxene. Based on the absence of Mg-rich cumulus orthopyroxene, they also suggested that these pressures are less than ~ 5 kbar. These qualitative estimates are supported by two-pyroxenes geobarometry (this work and Putirka, 2017) and *avP* calculations. The latter method also appears to detect a possible lithological variation with pressure. Looking closely at the *avP* results, ultramafic xenoliths are among those that record the highest pressures, troctolites and gabbronorites record lowest pressures and estimates for the ol-gabbros span almost over the entire range (Figs. 2b and 4).

This translates in a sequence of ultramafic xenoliths and ol-gabbros from 18 km to 11 km b.s.l., ol-gabbros and minor gabbronorites from ~11 km to ~ 3 km b.s.l. and gabbronorites and troctolites from ~ 3 km b.s.l. to the subsurface beneath the summit (Fig. 5).

4.2 Geobarometry of xenoliths as one of the links between petrology and geophysics

Seismic velocity and gravity modelling are indispensable to investigate the deep structure and physical properties of active magmatic systems and the lithosphere in which they emplace. They are known however to provide non-univocal solutions about the thermal state, chemistry and phase assemblages of the imaged geophysical bodies. The number of solutions can be significantly decreased if there is a xenolith cargo in the erupted lavas that can be combined to the geophysical information. Recent work on the Lesser Antilles and Aleutian arcs, for example, proved the potential of integrating the petrology of xenoliths to the seismic information (Kiddle et al., 2010; Melekhova et al., 2019; Shillington et al., 2004). In the following, I show a brief and simplified exercise comparing the xenolith data from Hualalai and Mauna Kea to one of the existing seismic models of the crust beneath Hawaii. In this exercise, it is important to bear in mind that xenoliths likely represent conduits and reservoirs with dike, sill or room shapes and variable sizes (Fodor & Galar, 1997), which might or might not be sufficiently large to be detected by seismic methods. For the sake of this exercise it is also assumed that the xenolith populations are, to some extent, representative of most of the lithologies in the subsurface of Hawaiian volcanoes.

Seismic properties (P-wave velocity – Vp, density - ρ) have been calculated for each xenolith using the model of Abers and Hacker (2016), at the temperatures $T_{\text{Ca-in-ol}}$ and pressures $\overline{P}$ calculated in this work. The model of Abers and Hacker (2016) calculates the physical properties of mineral assemblages at high pressures and temperature by applying Voigt–Reuss–Hill and Hashin–Shtrikman averages on the pure end-members of minerals. No melt, vapor phase or porosity are considered and the calculations do not take into account possible

anisotropy and anelastic or physical dispersion effects for finite-frequency signals (Abers & Hacker, 2016). The proportions of end-members were calculated from mineral proportions and compositions and therefore the calculations were limited to the xenoliths for which this information is available in the literature (Bohrson & Clague, 1988; Fodor & Galar, 1997; Fodor & Vandermeyden, 1988; Hoover & Fodor, 1997; Schamberger & Hammer, 2006). Results of the calculations are shown in Fig. 6. Calculated Vp vary in the range 6.8–7.2 km/s for gabbros, gabbronorites and diorites, 6.9–7.7 km/s for olivine-gabbros and 7.4–7.9 km/s for ultramafic xenoliths.

Figure 6 also compares 1D seismic profiles beneath southwestern Hualalai and southern Mauna Kea, extrapolated from the seismic tomography model of Park et al. (2009), to an ideal seismic profile built from room-temperature and high-pressure laboratory data of rock seismic properties (grey areas). The latter profile represents an ideal, end-member case in which the Hawaiian crust would be solely composed by shield-stage tholeiites on the top of the pre-Hawaiian oceanic crust (Fig. 5). If this was the real case beneath Hualalai and Mauna Kea, then the observed 1D seismic profiles should correspond to this ideal profile. Any positive variation from the ideality might indicate the presence of intrusions with higher Vp velocities and the Vp-depth relations of the xenoliths can help constraining the nature of these intrusions. Note that higher temperatures and the presence of melts or porosities would only decrease the Vp with respect to the experimental data.

At ~5–11 km depth beneath Hualalai, the seismic data of Park et al. (2009) shows velocities that are higher than those expected for Hawaiian tholeiites (Manghnani & Woollard, 1968), but lower than those calculated for the gabbro and gabbronorite xenoliths from similar depths (Fig. 6a). This might suggest that the depth interval 5–11 km beneath Hualalai is composed by shield-stage tholeiites variably intruded by gabbros and gabbronorite cumulates. Clearly, more gabbroic xenoliths need to be sampled and characterized to better define this depth interval.

Figure 6a also shows that the calculated Vp-depth relation of the ultramafic xenoliths from Hualalai (7.4–7.8 km/s) are consistent with the seismic tomography model of Park et al. (2009). This agreement supports the hypothesis that the dense, high-velocity bodies observed beneath the oceanic crust of Hawaiian islands (Watts et al., 1985) is indeed composed by intrusions of ultramafic cumulates (Clague, 1987; Richards et al., 2013). In the case of Hualalai, this intrusion might be as thick as ~3 km.

The depth interval 3–11 km beneath Mauna Kea shows a more pronounced disagreement between ideal (5.6–6.2 km/s) and observed (6.2–7.0 km/s) P wave velocities (Fig. 6b). The latter are much more consistent with the calculated velocities of xenoliths from the same depths (6.8–7.4 km/s), suggesting that a significant portion of the crust beneath Mauna Kea at 3–11 km depths have been intruded by basaltic magmas that fractionated to produced olivine-gabbros and minor gabbronorite cumulates. These lithologies could therefore be considered as the source of the high-velocity anomalies typically observed at these depths beneath Hawaiian volcanoes (e.g., Lin et al., 2014; Park et al., 2009). The presence of ol-gabbro and ultramafic xenoliths at 11–16 km depth suggests that the pre-Hawaiian oceanic crust at Mauna Kea has been more pervasively intruded by shield or postshield Hawaiian magmas, as opposed to Hualalai. However, the good agreement between observed and ideal seismic velocities and the significantly higher calculated velocities of the ultramafic lithologies, suggest that ultramafic cumulates are volumetrically less significant in this depth interval.

5 Conclusions and future perspectives

Mafic and ultramafic xenoliths in magmatic rocks are sporadic but valuable carriers of information about the physical and chemical structure of volcano plumbing systems. If from one hand they do not directly provide the spatial relationships of magmatic units as in the case of fossil crustal sections exposed at the surface (e.g., Ivrea-Verbano zone, southern Alps; Fountain & Salisbury 1981; Quick et al., 2009), on the other hand they represent the only direct

samples of deep solidified intrusions in active volcanic systems. This reason alone justifies the past and future petrological and geophysical studies characterizing the available xenoliths and the effort to model the temperatures and pressures recorded by their phase assemblages. The geothermobarometric study shown in this work is a small and simplified example of how this modelling can be approached.

Application of the *avP* method (Powell & Holland, 1994; Ziberna et al., 2017) to the gabbroic and ultramafic xenoliths from Hualalai and Mauna Kea produced pressure estimates with calculated uncertainties as low as 1.0 kbar, which allowed to detect some lithological variations with depth in these two volcanic systems (Fig. 5). Such estimates allowed also the xenolith data to be integrated with the available seismic models. Altogether, the results suggest that at Hualalai, ultramafic xenoliths likely represent fragments of one or more cumulate bodies intruded below the pre-Hawaiian oceanic crust. At Mauna Kea, on the other hand, ultramafic cumulate bodies might be less significant. Xenoliths of olivine-gabbros and ultramafic assemblages represent magmas that intruded and fractionated at shallower depths, within and above the pre-Hawaiian oceanic crust. A more in-depth work on a larger number of xenoliths will have to be performed to test these scenarios.

Despite this and other recent work (Cooper et al., 2019; Melekhova et al., 2017, 2019; Ziberna et al., 2017) demonstrate that conventional geothermobarometry of xenoliths can help unravelling important aspects about crustal magmatic systems, there are still issues that will need to be tackled in the future. For example, comparison between the results of two-pyroxenes and Ca-in-olivine geothermometry showed significant disagreement at low temperatures (< 1000˚C), which suggest that more experimental and theoretical work is needed to refine the phase equilibrium and diffusion models for mafic and ultramafic systems at subsolidus conditions. Differential diffusion of elements could influence not only the results of the above geothermometers, but also the results of a multiple-reaction method involving a significant

number of elements with potentially different diffusivities. At the same time, more work is needed to expand the application of the *avP* method to olivine-free magmatic rocks. This would allow the application of mutually consistent geothermobarometers to different xenoliths from the same populations and avoid possible inconsistency (compare Figs. 2a,b to Figs 2c,s). These observations confirm once more that geothermobarometry is a research field in continuous progress. Experimental and theoretical work refining the geothermobarometric models must proceed in parallel to their application to magmatic rocks and their xenoliths. Such an approach allows to identify and possibly solve relevant problems in geothermobarometry and therefore improve our knowledge about the complex architecture of magmatic systems.

Acknowledgments

The editors are thanked for their patience and helpful editorial handling and one anonymous reviewer is thanked for the constructive review. I also thank Angelo De Min and Francesco Narduzzi for the useful discussions.

References

Abers, G. A., & Hacker, B. R. (2016). A MATLAB toolbox and Excel workbook for calculating the densities, seismic wave speeds, and major element composition of minerals and rocks at pressure and temperature. *Geochemistry, Geophysics, Geosystems, 17*, 616-624. doi:10.1002/2015GC006171.

Baker, D. R., & Eggler, D. H. (1987). Compositions of anhydrous and hydrous melts coexisting with plagioclase, augite, and olivine or low-Ca pyroxene from 1 atm to 8 kbar: Application to the Aleutian volcanic center of Atka. *American Mineralogist, 72*, 12-28.

Baker, M. B., & Stolper, E. M. (1994). Determining the composition of high-pressure mantle melts using diamond aggregates. *Geochimica et Cosmochimica Acta, 58*, 2811-2827. https://doi.org/10.1016/0016-7037(94)90116-3.

Bartels, K. S., Kinzler, R. J., & Grove, T. L. (1991). High pressure phase relations of primitive high-alumina basalts from Medicine Lake volcano, northern California. *Contributions to Mineralogy and Petrology, 108*, 253-270. https://doi.org/10.1007/BF00285935.

Blatter, D. L., Sisson, T. W., & Hankins, W. B. (2013). Crystallization of oxidized, moderately hydrous arc basalt at mid- to lower-crustal pressures: Implications for andesite genesis.

Contributions to Mineralogy and Petrology, 166, 861-886. https://doi.org/10.1007/s00410-013-0920-3.

Blundy, J. D., & Holland, T. J. B. (1990). Calcic amphibole equilibria and a new amphibole-plagioclase geothermometer. *Contributions to Mineralogy and Petrology, 104*, 208-224.

Bohrson, W. A., & Clague, D. A. (1988). Origin of ultramafic xenoliths containing exsolved pyroxenes from Hualalai Volcano, Hawaii. *Contributions to Mineralogy and Petrology*, 100 (2), 139-155.

Borghini, G., Fumagalli, P., & Rampone, E. (2010). The stability of plagioclase in the upper mantle: subsolidus experiments on fertile and depleted lherzolite. *Journal of Petrology, 51*, 229-254. https://doi.org/10.1093/petrology/egp079.

Bowen, N. L. (1928). *The evolution of igneous rocks*. Princeton, NJ: Princeton Univ. Press.

Chakraborty, S. (2010). Diffusion coefficients in olivine, wadsleyite and ringwoodite. *Reviews in Mineralogy & Geochemistry, 72*(1), 603-639. https://doi.org/10.2138/rmg.2010.72.13.

Chalot-Prat, F., Falloon, T. J., Green, D. H., and &, W.O. (2010). An experimental study of liquid compositions in equilibrium with plagioclase + spinel lherzolite at low pressures (0.75 GPa). *Journal of Petrology, 51*, 2349-2376. https://doi.org/10.1093/petrology/egq060.

Chalot-Prat, F., Falloon, T. J., Green, D. H., and &, W.O. (2013). Melting of plagioclase + spinel lherzolite at low pressures (0.5 GPa): An experimental approach to the evolution of basaltic melt during mantle refertilisation at shallow depths. *Lithos, 172-173*, 61-80. https://doi.org/10.1016/j.lithos.2013.03.012.

Chen, C., Presnall, D. C., & Stern, R. J. (1992). Petrogenesis of ultramafic xenoliths from the 1800 Kaupulehu flow, Hualalai volcano, Hawaii. *Journal of Petrology, 33*(1), 163-202. https://doi.org/10.1093/petrology/33.1.163.

Cherniak, D. J., & Dimanov, A. (2010). Diffusion in pyroxene, mica and amphibole. *Reviews in Mineralogy & Geochemistry, 72*(1), 641-690. https://doi.org/10.2138/rmg.2010.72.14.

Christensen, N. I., & Mooney, W. D. (1995). Seismic velocity structure and composition of the continental crust: A global view. *Journal of Geophysical Research, 100*(B6): 9761-9788. https://doi.org/10.1029/95JB00259.

Clague, D. A. (1987). Hawaiian xenolith populations, magma supply rates, and development of magma chambers. *Bulletin of Volcanology, 49* (4), 577-587.

Clague, D. A. (1987). Hawaiian xenolith populations, magma supply rates and development of magma chambers. *Bulletin of Volcanology, 49*(4), 577-587. https://doi.org/10.1007/BF01079963.

Clague, D. A., & Bohrson, W. A. (1991). Origin of xenoliths in the trachyte at Puu Waawaa, Hualalai Volcano, Hawaii. *Contributions to Mineralogy and Petrology, 108*(4), 439-452. https://doi.org/10.1007/BF00303448

Clague, D. A., Jackson, E. D., & Wright, T. L. (1980). Petrology of Hualalai Volcano, Hawaii: implication for mantle composition. *Bulletin Volcanologique, 43*(4), 641-656. https://doi.org/10.1007/BF02600363.

Coogan, L. A., Hain, A., Stahl, S., & Chakraborty, S. (2005). Experimental determination of the diffusion coefficient for calcium in olivine between 900 °C and 1500 °C. *Geochimica et Cosmochimica Acta 69*(14), 3683-3694. https://doi.org/10.1016/j.gca.2005.03.002

Cooper, G. F., Blundy, D. J., Macpherson, C. G., Humbphreys, M. C. S., & Davidson, J. P. (2019). Evidence from plutonic xenoliths for magma differentiation, mixing and storage in a volatile-rich crystal mush beneath St. Eustatius, Lesser Antilles. *Contributions to Mineralogy and Petrology, 174*, 39. https://doi.org/10.1007/s00410-019-1576-4.

Cousens, B. L., Clague, D. A., & Sharp, W. D. (2003). Chronology, chemistry, and origin of trachytes from Hualalai Volcano, Hawaii. *Geochemistry Geophysics Geosystems, 4*(9), https://doi.org/10.1029/2003GC000560.

Di Carlo, I., Pichavant, M., Rotolo, S., & Scaillet, B. (2006). Experimental crystallization of a high-K arc basalt: The Golden Pumice, Stromboli Volcano (Italy). *Journal of Petrology, 47*, 1317-1343. https://doi.org/10.1093/petrology/egl011.

Droop, G. T. R. (1987) A general equation for estimation of Fe^{3+} concentrations in ferromagnesian silicates and oxides from microprobe analysis, using stoichiometry criteria. *Mineralogical Magazine, 51*, 431-435.

Erdmann, S., Martel, C., Pichavant, M., & Kushnir, A. (2014) Amphibole as an archivist of magmatic crystallization conditions: Problems, potential, and implications for inferring magma storage prior to the paroxysmal 2010 eruption of Mount Merapi, Indonesia. *Contributions to Mineralogy and Petrology, 167*, 1016. https://doi.org/10.1007/s00410-014-1016-4.

Feig, S. T., Koepke, J., & Snow, J. E. (2006). Effect of water on tholeiitic basalt phase equilibria: an experimental study under oxidizing conditions. *Contributions to Mineralogy and Petrology, 152*, 611-638. https://doi.org/10.1007/s00410-006-0123-2.

Feig, S. T., Koepke, J., & Snow, J. E. (2010). Effect of oxygen fugacity and water on phase equilibria of a hydrous tholeiitic basalt. *Contributions to Mineralogy and Petrology, 160*, 551-568. https://doi.org/10.1007/s00410-010-0493-3.

Fodor, R. V. & Galar, P. (1997). A view into the subsurface of Mauna Kea volcano, Hawaii: crystallization processes interpreted through the petrology and petrography of gabbroic and ultramafic xenoliths. *Journal of Petrology, 38* (5), 581-624. https://doi.org/10.1093/petroj/38.5.581.

Fodor, R. V., & Vandermeyden, H. J. (1988). Petrology of gabbroic xenoliths from Mauna Kea volcano, Hawaii. *Journal of Geophysical Research, 93*, 4435-4452. https://doi.org/10.1029/JB093iB05p04435.

Fodor, R.V. (2001). The role of tonalite and diorite in Mauna Kea Volcano, Hawaii, magmatism: petrology of summit-region leucocratic xenoliths. *Journal of Petrology, 42*, 1685-1704. https://doi.org/10.1093/petrology/42.9.1685.

Fountain, D. M., & Salisbury, M. H. (1981). Exposed cross-sections through the continental crust: implications for crustal structure, petrology, and evolution. *Earth and Planetary Science Letters, 56*, 263-277. https://doi.org/10.1016/0012-821X(81)90133-3.

Frey, F. A., Garcia, M. O., Wise, W. S., Kennedy, A., Gurriet, P., & Albarede, F. (1991). The evolution of Mauna Kea volcano, Hawaii: petrogenesis of tholeiitic and alkalic basalts.

Journal of Geophysical Research, 96, 14347-14375. https://doi.org/10.1029/91JB00940.

Frey, F. A., Wise, W. S., Garcia, M. O., West, H., Kwon, S. T., & Kennedy, A. (1990). Evolution of Mauna Kea volcano, Hawaii: petrologic and geochemical constraints on postshield volcanism. *Journal of Geophysical Research, 95,* 1271-1300. https://doi.org/10.1029/JB095iB02p01271.

Fumagalli, P., Borghini, G., Rampone, E., & Poli, S. (2017). Experimental calibration of Forsterite–Anorthite–Ca-Tschermak–Enstatite (FACE) geobarometer for mantle peridotites. *Contributions to Mineralogy and Petrology, 172*, 38. https://doi.org/10.1007/s00410-017-1352-2.

Gaetani, G. A., & Grove, T. L. (1998). The influence of water on melting of mantle peridotite. *Contributions to Mineralogy and Petrology, 131*, 323-346. https://doi.org/10.1007/s004100050396.

Gaetani, G. A., Grove, T. L., & Bryan, W. B. (1994). Experimental phase relations of basaltic andesite from Hole 839B under hydrous and anhydrous conditions. In J. Hawkins, L. Parson, J. Allan, et al. (Eds.), *Proceedings of the Ocean Drilling Program, Scientific Results, 135*.

Gao, R., Lassiter, J. C., Barnes, J. D., Clague, D. A., & Bohrson, W. A. (2016). Geochemical investigation of Gabbroic Xenoliths from Hualalai Volcano: Implications for lower oceanic crust accretion and Hualalai Volcano magma storage system. *Earth and Planetary Science Letters, 442*, 162-172. http://dx.doi.org/10.1016/j.epsl.2016.02.043.

Ghiorso, M. S., & R. O. Sack (1995). Chemical mass transfer in magmatic processes, IV, A revised and internally consistent thermodynamic model for the interpolation and extrapolation of liquid-solid equilibria in magmatic systems at elevated temperatures and pressures. *Contributions to Mineralogy and Petrology, 119*(2-3), 197-212. https://doi.org/10.1007/BF00307281.

Ghiorso, M.S., & Evans, B.W. (2008). Thermodynamics of rhombohedral oxide solid solutions and a revision of the Fe-Ti two-oxide geothermometer and oxygen-barometer. *American Journal of Science, 308*(9), 957–1039. https://doi.org/10.2475/09.2008.01.

Giacomoni, P. P., Coltorti, M., Bryce, J. G., Fahnestock, M. F., & Guitreau, M. (2016). Mt. Etna plumbing system revealed by combined textural, compositional, and thermobarometric studies in clinopyroxene. *Contributions to Mineralogy and Petrology, 171*, 34. https://doi.org/10.1007/s00410-016-1247-7.

Green, D.H., & Ringwood, A.E. (1967). The genesis of basaltic magmas. *Contributions to Mineralogy and Petrology, 15*, 103. https://doi.org/10.1007/BF00372052.

Grove, T. L., & Bryan, W. B. (1983). Fractionation of pyroxene-pyric MORB at low pressure: An experimental study. *Contributions to Mineralogy and Petrology, 84*, 293-309. https://doi.org/10.1007/BF01160283.

Grove, T. L., & Juster, T. C. (1989). Experimental investigations of low-Ca pyroxene stability and olivine–pyroxene–liquid equilibria at 1-atm in natural basaltic and andesitic liquids. *Contributions to Mineralogy and Petrology, 103*, 287-305. https://doi.org/10.1007/BF00402916.

Grove, T. L., Donnelly-Nolan, J. M., & Housh, T. (1997). Magmatic processes that generated the rhyolite of Glass Mountain, Medicine Lake volcano, N. California. *Contributions to Mineralogy and Petrology, 127*, 205-223. https://doi.org/10.1007/s004100050276.

Gualda, G. A. R., Ghiorso, M. S., Lemons, R. V., & Carley, T. L. (2012). Rhyolite- MELTS: a modified calibration of MELTS optimized for silica-rich, fluid-bearing magmatic systems. *Journal of Petrology, 53*(5), 875-890. https://doi.org/10.1093/petrology/egr080.

Hamada, M., & Fuji, T. (2008). Experimental constraints on the effects of pressure and H_2O on the fractional crystallization of high-Mg island arc basalt. *Contributions to Mineralogy and Petrology, 155*, 767-790. https://doi.org/10.1007/s00410-007-0269-6.

Holland, T. J. B., & Powell, R. (2011). An improved and extended internally-consistent thermodynamic dataset for phases of petrological interest, involving a new equation of state for solids. *Journal of Metamorphic Geology, 29*(3), 333-383. https://doi.org/10.1111/j.1525-1314.2010.00923.x.

Holland, T., & Blundy, J. (1994). Non-ideal interactions in calcic amphiboles and their bearing on amphibole-plagioclase thermometry. *Contributions to Mineralogy and Petrology, 116*, 433–447. https://doi.org/10.1007/BF00310910.

Hoover, S. R., & Fodor, R. V. (1997). Magma-reservoir crystallization processes: small-scale dikes in cumulate gabbros, Mauna Kea volcano, Hawaii. *Bulletin of Volcanology, 59*(3), 186-197. https://doi.org/10.1007/s004450050185.

Huang, S., & Frey, F. A. (2003). Trace element abundances of Mauna Kea basalt from phase 2 of the Hawaii Scientific Drilling Project: Petrogenetic implications of correlations with major element content and isotopic ratios. *Geochemistry, Geophysics, Geosystems, 4*, paper 2002GC000322. https://doi.org/10.1029/2002GC000322.

Husen, A., Almeev, R. R., & Holtz, F. (2016). The effect of H_2O on pressure and multiple saturation and liquid line of descent in basalt from the Shatsky Rise. *Journal of Petrology, 57*, 309-344. https://doi.org/10.1093/petrology/egw008.

Jackson, E. D., Beeson, M. H., & Clague, D. A. (1982). Xenoliths in volcanics from Mauna Kea Volcano, Hawaii. USGS Open-File Report, 82-201. https://doi.org/10.3133/ofr82201.

Jackson, E. D., Clague, D. A., Engleman, E., Friesen, W. F., & Norton, D. (1981). Xenoliths in the alkalic basalt flows from Hualalai Volcano, Hawaii. USGS *Open-File Report, 81-1031*. https://doi.org/10.3133/ofr811031.

Jennings, E. S. & Holland, T. J. B. 2015. A simple thermodynamic model for melting of peridotite in the system NCFMASOCr. *Journal of Petrology, 56*, 869-892. https://doi.org/10.1093/petrology/egv020.

Khazanehdari, J., Rutter, E. H., & Brodie, K. H. (2000). High-pressure-high-temperature seismic velocity structure of the midcrustal and lower crustal rocks of the Ivrea-Verbano zone and Serie dei Laghi, NW Italy. *Journal of Geophysical Research, 105*(B6), 13843-13858. https://doi.org/10.1029/2000JB900025.

Kiddle, E. J., Edwards, B. R., Loughlin, S. C., Petterson, M., Sparks, R. S. J., & Voight, B. (2010). Crustal structure beneath Montserrat, Lesser Antilles, constrained by xenoliths, seismic velocity structure and petrology. *Geophysical Research Letters, 37*(19). https://doi.org/10.1029/ 2009GL042145.

Kinzler, R. J., & Grove, T. L. (1992). Primary magmas of Mid-Ocean Ridge Basalts 1. Experiments and methods. *Journal of Geophysical Research, 97*, 6885-6906.

Köhler, T. P., & Brey, G. P. (1990). Calcium exchange between olivine and clinopyroxene calibrated as a geothermobarometer for natural peridotites from 2 to 60 kbar with applications. *Geochimica et Cosmochimica Acta, 54*, 2375-2388.

Lambart, S., Laporte, D., & Schiano, P. (2009). An experimental study of focused magma transport and basalt–peridotite interactions beneath mid-ocean ridges: implications for the generation of primitive MORB compositions. *Contributions to Mineralogy and Petrology, 157*, 429-451. https://doi.org/ 10.1007/s00410-008-0344-7.

Lange, R. A., Frey, H. M., & Hector, J. (2009). A thermodynamic model for the plagioclase-liquid hygrometer/thermometer. *American Mineralogist, 94*(4), 494-506. https://doi.org/10.2138/am.2009.3011.

Lanzo, G., Di Carlo, I., Pichavant, M., Rotolo, S. G., & Scaillet, B. (2016). Origin of primitive ultra-calcic arc melts at crustal conditions — Experimental evidence on the La Sommata basalt, Vulcano, Aeolian Islands. *Journal of Volcanology and Geothermal Research, 321*, 85-101. http://dx.doi.org/10.1016/j.jvolgeores.2016.04.032.

Laporte, D., Toplis, M. J., Seyler, M., & Devidal, J.-L. (2004). A new experimental technique for extracting liquids from peridotite at very low degrees of melting: application to partial melting of depleted peridotite. *Contributions to Mineralogy and Petrology, 146*, 463-484. https://doi.org/10.1007/s00410-003-0509-3.

Liang, Y., Sun, C. & Yao, L. (2013). A REE-in-two-pyroxene thermometer for mafic and ultramafic rocks. *Geochimica et Cosmochimica Acta, 102*, 246-260. https://doi.org/10.1016/j.gca.2012.10.035.

Lin, G., Shearer, P. M., Matoza, R. S., Okubo, P. G., & Amelung, F. (2014). Three-dimensional seismic velocity structure of Mauna Loa and Kilauea volcanoes in Hawaii from local seismic tomography. *Journal of Geophysical Research Solid Earth, 119*, 4377-4392, doi:10.1002/2013JB010820.

Lindsley, D. (1983). Pyroxene thermometry. *American Mineralogist, 68*(5-6), 477-493.

Manghnani, M. H., & Woollard, G. P. (1968). Elastic wave velocities in Hawaiian rocks at pressures to ten kilobars. *American Geophysisical Union Geophysical Monographs, 12*, 501-516. https://doi.org/10.1029/GM012p0501.

Masotta, M., Mollo, S., Freda, C., Gaeta, M., & Moore, G. (2013). Clinopyroxene–liquid thermometers and barometers specific to alkaline differentiated magmas. *Contributions to Mineralogy and Petrology, 166,* 1545-1561. https://doi.org/10.1007/s00410-013-0927-9.

Melekhova, E., Blundy, J., Martin, R., Arculus, R., & Pichavant, M. (2017). Petrological and experimental evidence for differentiation of water-rich magmas beneath St. Kitts, Lesser Antilles. *Contributions to Mineralogy and Petrology, 172*, 98. https://doi.org/10.1007/ s00410- 017- 1416- 3.

Melekhova, E., Blundy, J., Robertson, R., & Humphreys, M. C. S. (2015). Experimental evidence for polybaric differentiation of primitive arc basalt beneath St. Vincent, Lesser Antilles. *Journal of Petrology, 56,* 161-192. https://doi.org/10.1093/petrology/egu074.

Melekhova, E., Schlaphorst, D., Blundy, J., Kendall, J. M., Connolly, C., McCarthy, A., & Arculus, R. (2019). Lateral variation in crustal structure along the Lesser Antilles arc from petrology of crustal xenoliths and seismic receiver functions. *Earth and Planetary Science Letters, 516*, 12-24. https://doi.org/10.1016/j.epsl.2019.03.030.

Molina, J. F., Moreno, J. A., Castro, A., Rodruiguez, C., & Fershtater, G. B. (2015). Calcic amphibole thermobarometry in metamorphic and igneous rocks: new calibrations based on plagioclase/amphibole Al-Si partitioning and amphibole-liquid Mg partitioning. *Lithos, 232*, 286-305. https://doi.org/10.1016/j.lithos.2015.06.027.

Mollo, S., Blundy, J., Scarlato, P., De Cristofaro, S.P., Tecchiato, V., Di Stefano, F., Vetere, F., Holtz F., & Bachmann, O. (2018). An integrated P-T-H2O-lattice strain model to quantify the role of clinopyroxene fractionation on REE+Y and HFSE patterns of mafic alkaline magmas: Application to eruptions at Mt. Etna. *Earth-Science Reviews, 185*, 32-56. https://doi.org/10.1016/j.earscirev.2018.05.014.

Mollo, S., Giacomoni, P. P., Coltorti, M., Ferlito, C., Iezzi, G., & Scarlato, P. (2015). Reconstruction of magmatic variables governing recent Etnean eruptions: constraints from mineral chemistry and P-T-fO_2-H_2O modelling. *Lithos, 212-215*, 311-320. https://doi.org/10.1016/j.lithos.2014.11.020.

Mollo, S., Ubide, T., Di Stefano, F., Nazzari, M. & Scarlato, P. (2020). Polybaric/polythermal magma transport and trace element partitioning recorded in single crystals: A case study of a zoned clinopyroxene from Mt. Etna. *Lithos*. https://doi.org/10.1016/j.lithos.2020.105382.

Moore, R. B., Clague, D. A., Meyer, R., & Bohrson, W. A. (1987). Hualālai Volcano: A preliminary summary of geologic, petrologic and geophysical data. In R. W. Decker, T.L. Wright, P. H. Stauffer (Eds.), *Volcanism in Hawaii*. USGS Professional Paper 1350, 571-585.

Müller, T., Dohmen, R., Becker, H. W., ter Heege, J. H., & Chakraborty, S. (2013). Fe–Mg interdiffusion rates in clinopyroxene: experimental data and implications for Fe–Mg exchange geothermometers. *Contributions to Mineralogy and Petrology, 166*(6), 1563-1576. https://doi.org/10.1007/s00410-013-0941-y.

Nandedkar, R. H., Ulmer, P., & Müntener, O. (2014). Fractional crystallization of primitive, hydrous arc magmas: an experimental study at 0.7 GPa. *Contributions to Mineralogy and Petrology, 167*, 1015. https://doi.org/ 10.1007/s00410-014-1015-5.

Neave, D. A., & Putirka, K. D. (2017). A new clinopyroxene-liquid barometer, and implications for magma storage pressures under Icelandic rift zones. *American Mineralogist, 102*(4), 777-794. https://doi.org/10.2138/am-2017-5968.

Neave, D. A., Bali, E., Guðfinnsson, G. H., Halldórsson, S. A., Kahl, M., Schmidt, A.-S., & Holtz, F. (2019). Clinopyroxene–liquid equilibria and geothermobarometry in natural and experimental tholeiites: the 2014–2015 Holuhraun eruption, Iceland, *Journal of Petrology, egz042*, https://doi.org/10.1093/petrology/egz042.

Nimis, P. (1999). Clinopyroxene geobarometry of magmatic rocks: part 2—structural geobarometers for basic to acid, tholeiitic and mildly alkaline magmatic systems. *Contributions to Mineralogy and Petrology, 135*(1), 62-74. https://doi.org/10.1007/s004100050498.

Parat, F., Streck, M. J., Holtz, F., & Almeev, R. (2014). Experimental study into the petrogenesis of crystal-rich basaltic to andesitic magmas at Arenal volcano. *Contributions to Mineralogy and Petrology, 168*, 1040. https://doi.org/10.1007/s00410-014-1040-4.

Park, J., Morgan, J. K., Zelt, C. A., & Okubo, P. G. (2009). Volcano-tectonic implications of 3-D velocity structures derived from joint active and passive source tomography of the

island of Hawaii, *Journal of Geophysical Research, 114*, B09301, https://doi.org/10.1029/2008JB005929.

Pichavant, M., & Macdonald, R. (2007). Crystallization of primitive basaltic magmas at crustal pressures and genesis of the calc-alkaline igneous suite: experimental evidence from St Vincent, Lesser Antilles arc. *Contributions to Mineralogy and Petrology, 154*, 535-558. https://doi.org/10.1007/s00410-007-0208-6.

Powell, R., & Holland, T. J. B. (1994). Optimal geothermometry and geobarometry. *American Mineralogist, 79*(1-2), 120-133.

Putirka, K. D. (2008). Thermometers and barometers for volcanic systems. *Reviews in Mineralogy and Geochemistry, 69*, 61-120. https://doi.org/10.2138/rmg.2008.69.3

Putirka, K. (1997). Magma transport at Hawaii: inferences from igneous thermobarometry. *Geology, 25*, 69-72. https://doi.org/10.1130/0091-7613(1997)025<0069.

Putirka, K. (2016). Amphibole thermometers and barometers for igneous systems and some implications for eruption mechanisms of felsic magmas at arc volcanoes. *American Mineralogist, 101*(4), 841-858. https://doi.org/10.2138/am-2016-5506.

Putirka, K. (2017). Down the crater: Where magmas are stored and why they erupt. Elements, 13, 11-16. https://doi.org/10.2113/gselements.13.1.11

Quick, J. E., Sinigoi, S., Peressini, G., Demarchi, G., Wooden, J. L. & Sbisà, A. (2009). Magmatic plumbing of a large Permian caldera exposed to a depth of 25 km. *Geology 37*, 603-606. https://doi.org/10.1130/G30003A.1.

Richards, M., Contreras-Reyes, E., Lithgow-Bertelloni, C., Ghiorso, M., & Strixrude, L. (2013). Petrological interpretation of deep crustal intrusive bodies beneath oceanic hotspot provinces. *Geochemistry, Geophysics, Geosystems, 14*(3), 604-619, https://doi.org/10.1029/2012GC004448.

Shamberger, P. J., & Hammer, J. E. (2006). Leucocratic and gabbroic xenoliths from Hualalai Volcano, Hawaii. *Journal of Petrology, 47*(9), 1785-1808. https://doi.org/10.1093/petrology/egl027.

Shejwalkar, A., & Coogan, L. A. (2013). Experimental calibration of the roles of temperature and composition in the Ca-in-olivine geothermometer at 0.1 MPa. *Lithos, 177*, 54-60. https://doi.org/10.1016/j.lithos.2013.06.013.

Shillington, D. J., Van Avendonk, H. J. A., Holbrook, W. S., Kelemen, P. B., & Hornbach, M. J. (2004). Composition and structure of the central Aleutian island arc from arc-parallel wide-angle seismic data. *Geochemistry, Geophysics, Geosystems, 5*(10), https://doi.org/10.1029/2004GC000715.

Sisson, T. W., & Grove, T. L. (1993). Experimental investigations of the role of H_2O in calc-alkaline differentiation and subduction zone magmatism. *Contributions to Mineralogy and Petrology, 113*, 143-166. https://doi.org/10.1007/BF00283225.

Stamper, C. C., Melekhova, E., Blundy, J. D., Arculus, R. J., Humphreys, M. C. S., & Brooker, R. A. (2014). Oxidised phase relations of a primitive basalt from Grenada, Lesser Antilles. *Contributions to Mineralogy and Petrology, 167*, 1-20. https://doi.org/10.1007/s00410-013-0954-6.

Stock, M. J., Bagnardi, M., Neave, D. A., Maclennan, J., Bernard, B., Buisman, I., et al. (2018). Integrated petrological and geophysical constraints on magma system architecture in

the western Galápagos Archipelago: Insights from Wolf volcano. *Geochemistry, Geophysics, Geosystems, 19*, 4722-4743. https://doi. org/10.1029/2018GC007936.

Streckeisen, A. (1976). To each plutonic rock its proper name. *Earth Science Reviews, 12*(1), 1-33.

Sun, C., & Liang, Y. (2015). A REE-in-garnet-clinopyroxene thermobarometer for eclogites, granulites and garnet peridotites. *Chemical Geology, 393*, 79-92. https://doi.org/10.1016/j.chemgeo.2014.11.014.

Sun, C., & Liang, Y. (2017). A REE-in-plagioclase–clinopyroxene thermometer for crustal rocks. *Contributions to Mineralogy and Petrology, 172*, 24. https://doi.org/10.1007/s00410-016-1326-9.

Tormey, D. R., Grove, T. L., & Bryan, W. B. (1987). Experimental petrology of normal MORB near the Kane Fracture Zone: 22˚–25˚, mid-Atlantic ridge. *Contributions to Mineralogy and Petrology, 96,* 121-139. https://doi.org/10.1007/BF00375227.

Tuttle, O. F., & Bowen, N. L. (1958). The origin of granite in the light of experimental studies in the system $NaAlSi_3O_8$- $KAlSi_3O_8$-SiO_2-H_2O. *Geological Society of America, 74*. https://doi.org/10.1130/MEM74.

Vazquez, J. A., Shamberger, P. J., & Hammer, J. E. (2007). Plutonic xenoliths reveal the timing of magma evolution at Hualalai and Mauna Kea, Hawaii. Geology, 35(8), 695-698. https://doi.org/10.1130/G23495A.1.

Watts, A. B., ten Brink, U. S., Buhl, P., & Brocher, T. M. (1985). A multichannel seismic study of lithospheric flexure across the Hawaiian-Emperor seamount chain. *Nature, 315*, 105-111.

Wells, P. R. A. (1977). Pyroxene thermometry in simple and complex systems. *Contributions to Mineralogy and Petrology, 62*(2), 129-139.

Wolfe, E. W., Wise, W. S., & Dalrymple, G. B. (1997). The geology and petrology of Mauna Kea volcano, Hawaii—a study of postshield volcanism. *US Geological Survey Professional Paper 1557*. https://doi.org/10.3133/pp1557.

Yang, H.-J., Kinzler, R. J., & Grove, T. L. (1996). Experiments and models of anhydrous, basaltic olivine-plagioclase-augite saturated melts from 0.001 to 10 kbar. *Contributions to Mineralogy and Petrology, 124*, 1-18. https://doi.org/10.1007/s004100050169.

Ziberna, L., Green, E. C. R., & Blundy, J. D. (2017). Multiple-reaction geobarometry for olivine-bearing igneous rocks. *American Mineralogist, 102*, 2349-2366. http://dx.doi.org/10.2138/am-2017-6154.

Zucca, J. J., Hill, D. P., & Kovach, R. L. (1982). Crustal structure of Mauna Loa volcano, Hawaii, from seismic refraction and gravity data. *Bulletin of the Seismological Society of America, 72*(5), 1535-1550.

Figure captions

Figure 1. Location of Hualalai and Mauna Kea volcanoes, Island of Hawaii. Background map is from Google Earth®, version 7.3.2.5776, imagery date 12/14/2015, eye altitude 265 km. Dashed line A-A' shows the position of the cross-section in Fig. 5.

Figure 2. Pressure and temperature estimates for (a,c) Hualalai and (b,d) Mauna Kea xenoliths using either (a,b) the *avP* method refined for SCOlP assemblage (Ziberna et al., 2017) ($\overline{P}$) combined with the Ca-in-olivine geothermometer of Shejwalkar and Coogan (2013) ($T_{Ca\text{-}in\text{-}ol}$) or (b,d) the two-pyroxenes geothermometer and geobarometer of Putirka et al. (2008) (his eqs. 39 – $P^{Cpx\text{-}Opx}$ and 36 – $T_{Cpx\text{-}Opx}$). Error bars in (a,b) are uncertainties ($\sigma_{\overline{P}}$) calculated through the *avP* algorithm, while errors in (c,d) are model errors as reported in Putirka (2008). Rock nomenclatures follow Streckeisen (1976).

Figure 3. Comparison between the results of Ca-in-olivine ($T_{Ca\text{-}in\text{-}ol}$; Shejwalkar & Coogan, 2013; SC13) and two-pyroxenes geothermometry ($T_{cpx\text{-}opx}$; Putirka, 2008). (a) Application to the xenoliths from Mauna Kea and Hualalai, using eq. 36 in Putirka (2008) and either eq. 12 (solid symbols) or eq. 13 (transparent symbols) in Shejwalkar and Coogan (2013). (b) Test of eq. 36 in Putirka (2008) and (c) Ca-in-olivine geothermometers using the experimental dataset collected in this study (Baker & Eggler, 1987; Baker & Stolper, 1994; Bartels et al., 1991; Blatter et al., 2013; Borghini et al., 2010; Chalot-Prat et al., 2010, 2013; Di Carlo et al., 2006; Feig et al., 2006, 2010; Gaetani & Grove, 1998; Gaetani et al., 1994; Grove & Juste, 1989; Grove et al., 1997; Grove & Bryan, 1983; Hamada & Fuji, 2008; Husen et al., 2016; Kinzler & Grove, 1992; Lambart et al., 2009; Lanzo et al., 2016; Laporte et al., 2004; Melekhova et al., 2015; Nandedkar et al., 2014; Parat et al., 2014; Pichavant & MacDonald, 2007; Sisson & Grove, 1993; Stamper et al., 2014; Tormey et al., 1987; Yang et al., 1996); only clinopyroxene+olivine-bearing experimental products were considered. (d) Deviations of Ca-in-olivine from experimental temperatures as a function of experimental pressures, for the same experimental dataset.

Figure 4. Pressure estimates for each Mauna Kea and Hualalai xenolith based on different sets of geothermobarometers. Errors are not shown for the sake of clarity of the plot. Dun – Dunite, Weh – Wehrlite, Ol-C – Olivine-clinopyroxenite, Ol-Web – Olivine-websterite, Ol-G, Olivine-gabbro, Troc – Troctolite, Ox-G – Oxide-gabbro, G – Gabbro, GN – Gabbronorite, Ol-GN – Olivine-gabbronorite, Hb-G – Hornblende-gabbro, Dio – Diorite, M-Dio – Monzodiorite, SG – Syenogabbro.

Figure 5. Schematic cross section of the island of Hawaii along the profile A-A' in Fig. 1 and tentative representation of the lithological variations beneath Hualalai and Mauna Kea (coloured boxes), based on *avP* calculations on the available xenoliths containing the assemblage SCOlP (see text). The colour code of the lithologies is the same as in Figs. 2 and 3. The range of calculated P-wave velocities and densities of each group of lithologies are also reported. The approximate ranges of Vp and ρ for tholeiites, oceanic crust and lithospheric mantle are from Christensen and Mooney (1995) and Manghnani and Woollard (1968). The grey cap on Hualalai and Mauna Kea does not represent the actual thickness of the postshield alkali basalts and is only shown as a sketch representation. Surface topography and depths of pre-Hawaiian oceanic crust are from Wolfe et al. (1997). Depths have been calculated from $\overline{P}$ assuming a constant density value of 3.0 g/cm^3.

Figure 6. Calculated P-wave velocities (Vp) vs. depth for the xenoliths from (a) Hualalai and (b) Mauna Kea. Depths have been calculated as in Fig. 5. Solid curves are 1D seismic profiles beneath south-eastern Hualalai and southern Mauna Kea extrapolated from the seismic tomography model of Park et al. (2009). Grey areas show the range of Vp measured in laboratory experiments (Behn & Kelemen, 2003; Khazanehdari et al., 2000; Manghnani & Woollard, 1968) for the rock types that are assumed to compose the hypothetical cross section in Fig.5, devoid of the cumulates represented by the xenoliths.

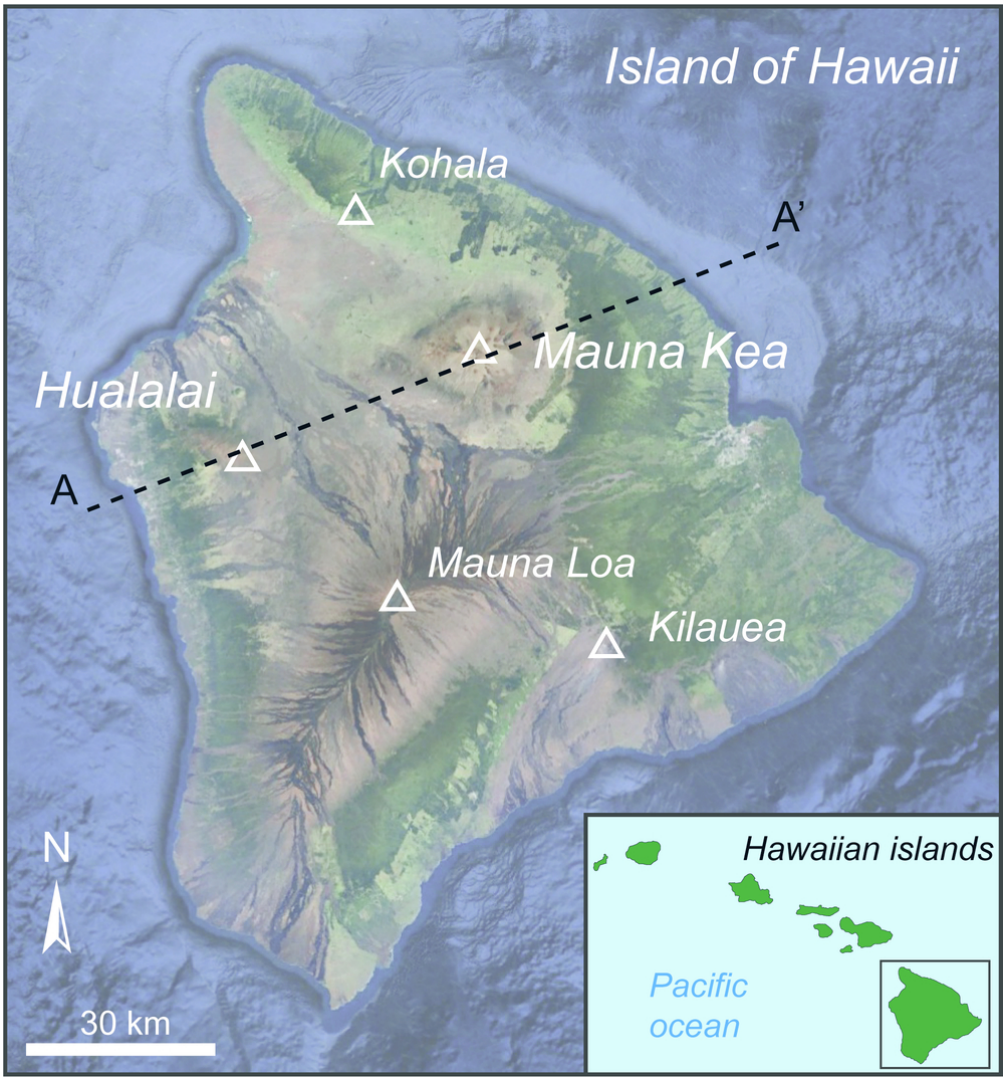

Figure 1

84x90mm (300 x 300 DPI)

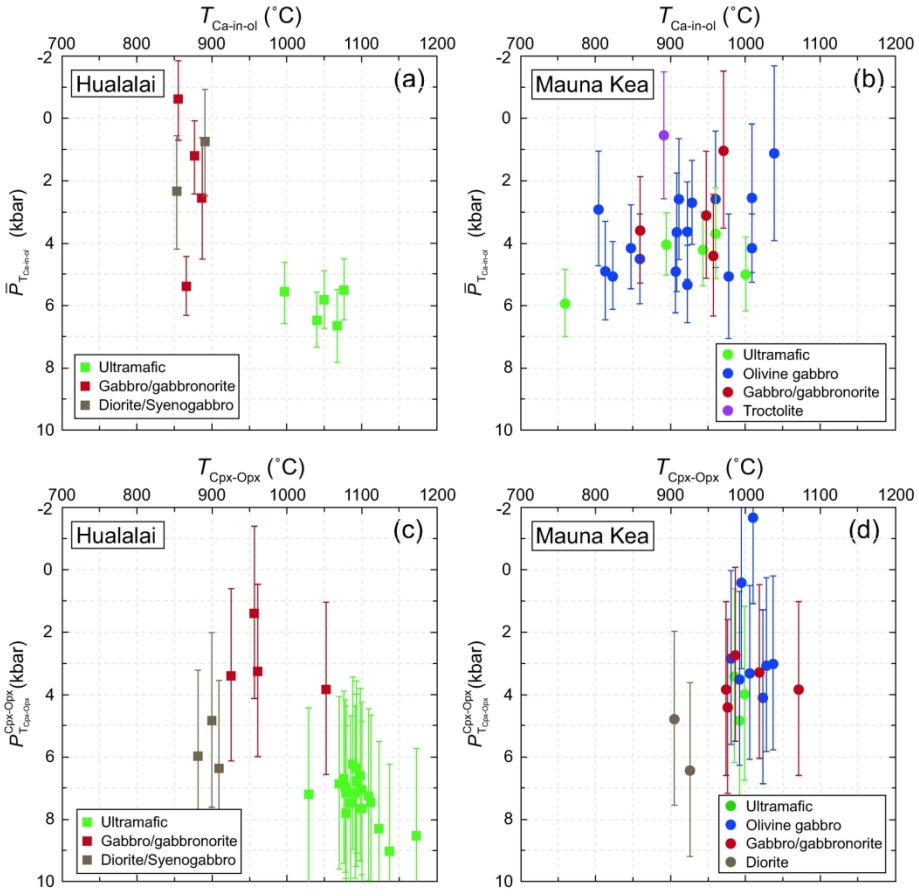

Figure 2

190x201mm (300 x 300 DPI)

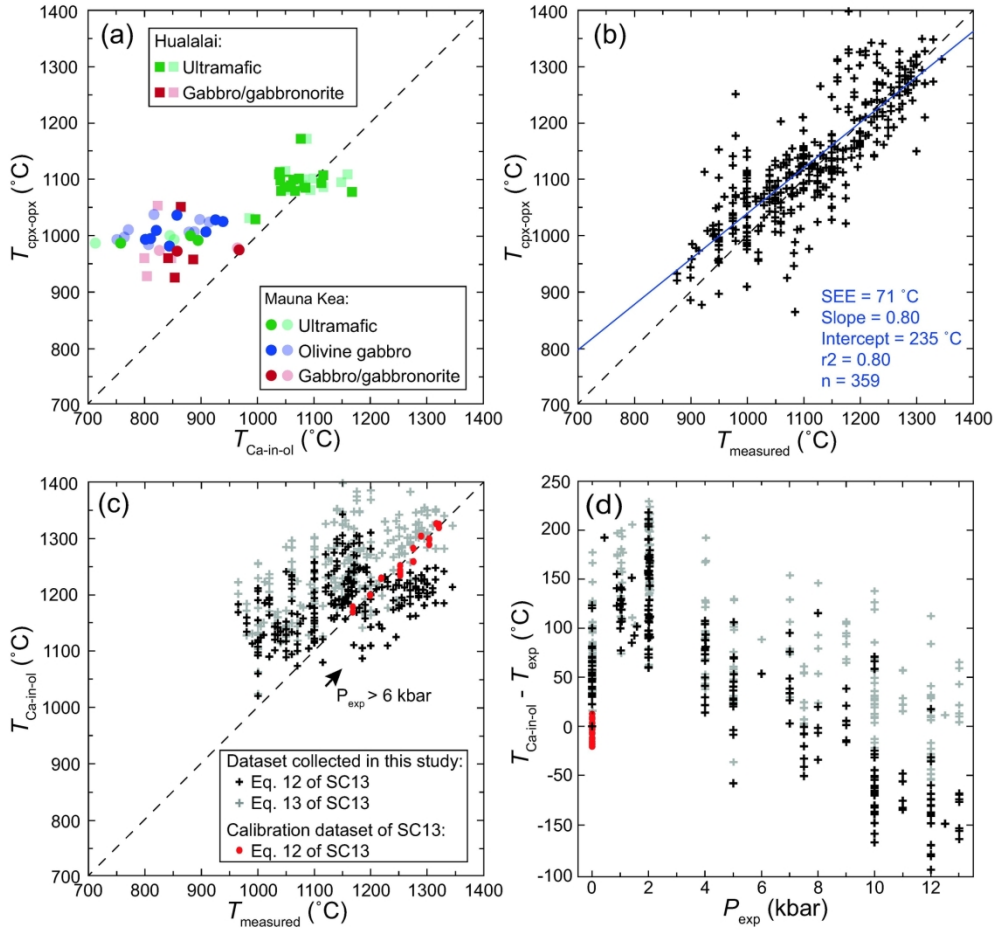

Figure 3

180x170mm (300 x 300 DPI)

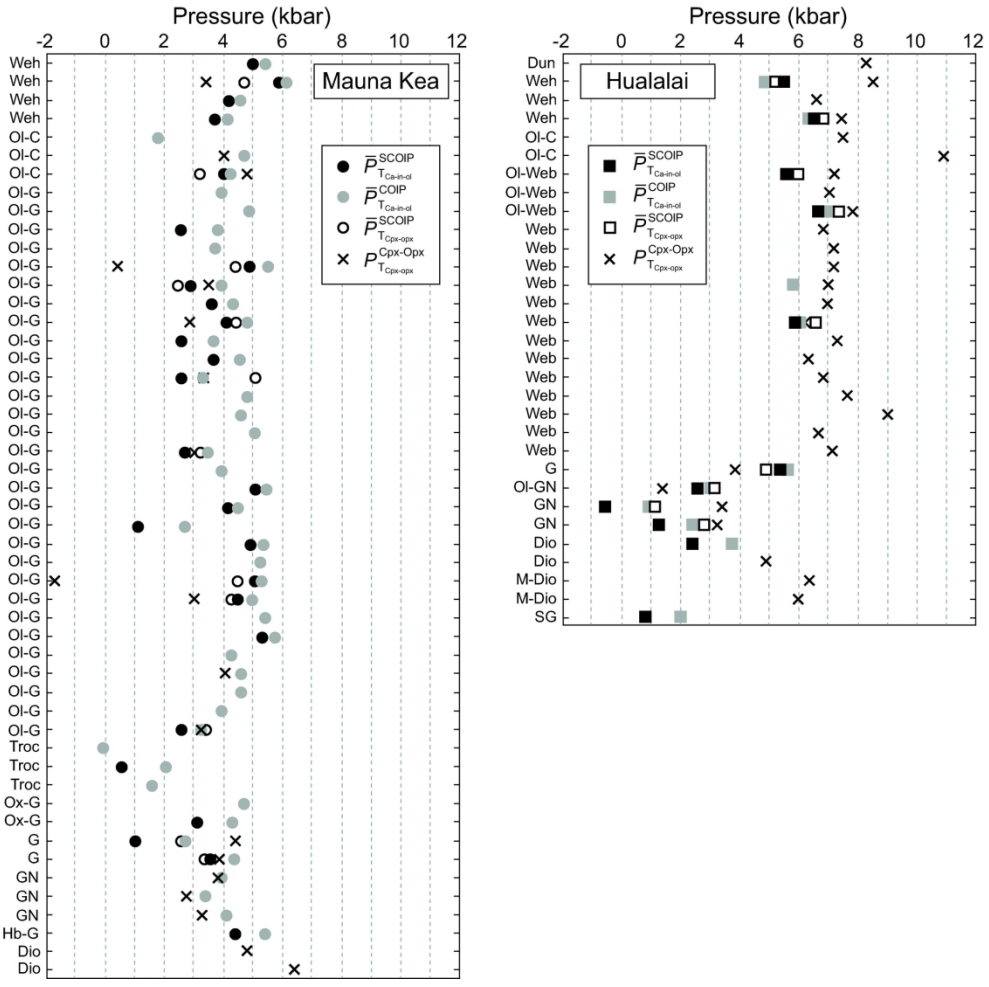

Figure 4

184x179mm (300 x 300 DPI)

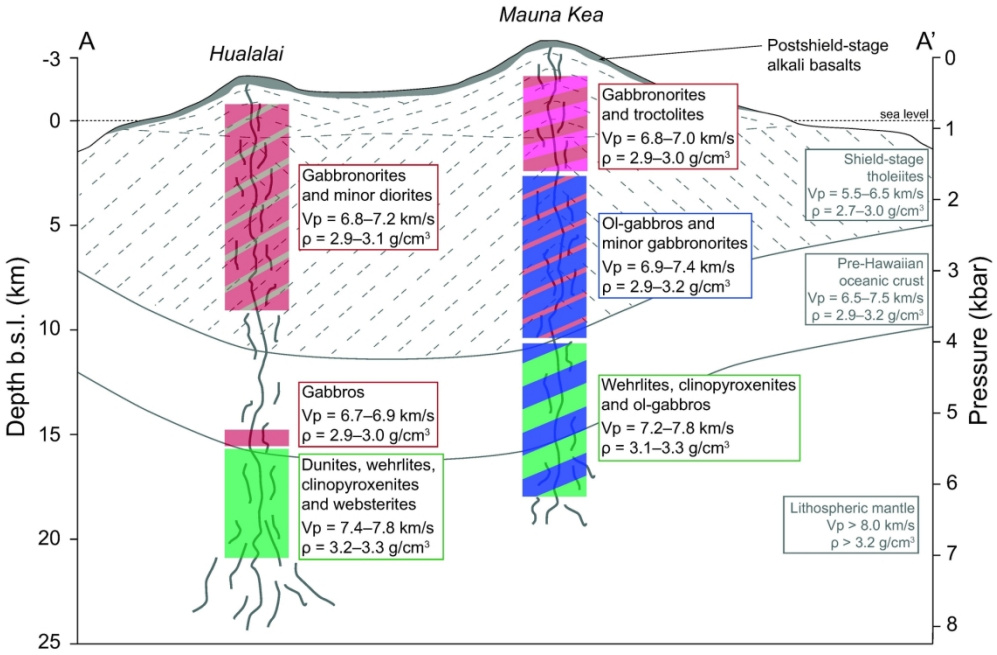

Figure 5

171x113mm (300 x 300 DPI)

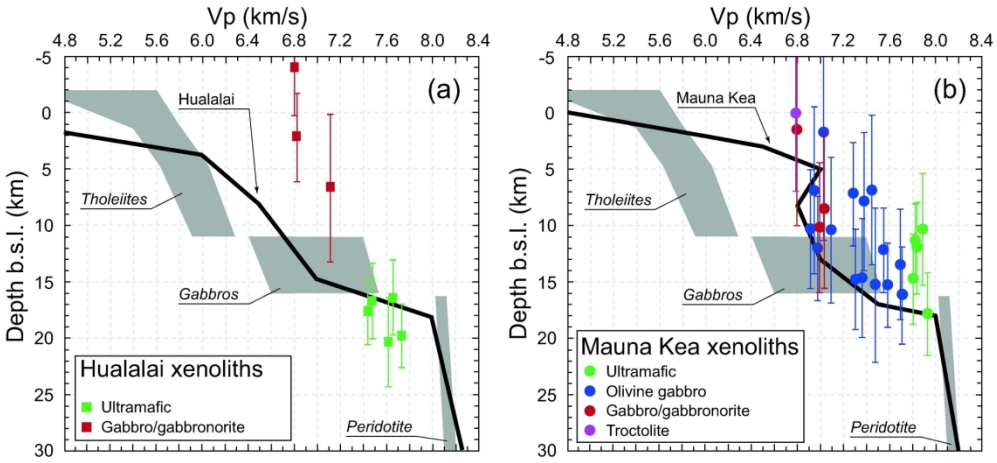

Figure 6

180x91mm (300 x 300 DPI)